Coherent neutron scattering response from glassy glycerol

J. Dawidowski,[1] F. J. Bermejo,[1] R. Fayos,[1] R. Fernández Perea,[1] S. M. Bennington,[2] and A. Criado[3]
[1]*Instituto de Estructura de la Materia, Consejo Superior de Investigaciones Científicas, Serrano 123, E-28006 Madrid, Spain*
[2]*ISIS Pulsed Neutron Facility, Rutherford Appleton Laboratory, Chilton, Didcot, Oxon, OX110QX, United Kingdom*
[3]*Departamento de Física de la Materia Condensada e Instituto de Ciencia de Materiales de Sevilla, Consejo Superior de Investigaciones Científicas, Box 1065, E-41080 Sevilla, Spain*

(Received 21 November 1995; revised manuscript received 12 January 1996)

We report on inelastic neutron scattering measurements of fully deuterated glassy glycerol at temperatures between 15 K to 180 K. Incident energies of 40 and 100 meV and momentum transfers up to ≈ 12 Å^{-1} were used. Analysis of the static structure factor calculated as the zeroth-frequency moment of $S(Q,\omega)$ enabled us to derive valuable structural information on the intra- and intermolecular correlations. Generalized frequency distributions are derived from the spectra and are used to calculate the relevant thermodynamic properties of the material using a quasiharmonic approximation. Estimates are also made for the first order anharmonic effects. Some wave-vector-dependent effects, such as the reduced frequency moments of $S(Q,\omega)$ are also evaluated, and their physical meaning discussed in some detail. [S1063-651X(96)03405-8]

PACS number(s): 61.25.Em, 65.40.+g, 61.43.Fs, 63.50.+x

I. INTRODUCTION

During the last decades a good number of studies regarding the dynamics of supercooled liquids and the glass transition as monitored by several means (static and dynamic specific heat measurements [1–3], optical relaxation studies [4, 5]) have been carried out using glycerol as a benchmark material. It shows a calorimetric liquid-glass transition at $T_g = 185$ K, and exhibits a very low rate of nucleation formation, making amenable its study within the supercooled state over long periods of time. However, it suffices to see most of the work carried out in recent times to realize the dearth of available information regarding structural and dynamic correlations at microscopic scales. Notable exceptions to this are constituted by some diffraction work [6–8], as well as computer molecular dynamics simulations [9]. The information derived from the former set of studies is, however, somewhat inconclusive due to a number of assumptions introduced to simplify the analysis of the diffraction patterns [10], and on the other hand, the computer calculations were carried out using a rather small system size (32 molecules in a cubic cell) thus making difficult a direct comparison with experimental magnitudes. In particular, significant difficulties were encountered when trying to separate inter- and intramolecular correlations from the experimental diffraction pattern. However it is the very peculiar behavior of such material, that is, its strongly enhanced stability once supercooled and relatively large viscosity when compared with other low molecular weight materials, which provides a rather direct indication of the relevant role of interparticle interactions. In fact, such distinctive behavior, has been noticed even at mesoscopic scales as explored by light scattering [11–13] and dielectric relaxation [14], where in contrast with other materials, significant deviations from the idealized simple liquid behavior have been reported. Our aim is thus to contribute towards the knowledge of the underlying microscopic forces which drive such an anomalous behavior by means of the study of some static and dynamical properties at scales of a few picoseconds and angstroms.

In this work, we report on the inelastic neutron scattering data on the glassy deuterated glycerol, from which we extract wave-vector-dependent structural and dynamical information. From the structural data, the information regarding static correlations is referred to that of the crystalline phase calculated from lattice dynamics, as well as with previous experimental data for the liquid phase. We also derive structural molecular parameters that are free from some of the uncertainties that riddled previous measurements. The dynamics of the glassy phase are compared with results regarding the orientationally averaged excitations occurring in the parent crystal [15]. Connection with macroscopic measurements is made through the calculation of the constant pressure specific heat which is compared with calorimetric measurements, with special attention paid to the anharmonic contributions. These results on the thermal properties are an extension of those reported in a previous communication [15]. In the earlier measurements a hydrogenous sample was used so that only incoherent scattering was recorded, and the measurement was made over a much smaller range of frequencies. On the other hand, the present measurements extend those of Wuttke *et al.* [13] to higher frequencies and wave-vectors as far as the glassy solid is concerned, a fact that in conjunction with the availability of an absolute frequency scale provided by the crystal frequency distribution serves to assign some of the features in the generalized frequency distributions discussed by those authors.

II. EXPERIMENTAL DETAILS AND DATA PROCESSING

The experiment was carried out on the MARI spectrometer at the ISIS pulsed neutron source at the Rutherford Appleton Laboratory in Oxfordshire. The sample was made of deuterated glycerol and the glassy solid was produced by a fast thermal quench of the room temperature liquid. The sample holder was a cylindrical annulus made of aluminum with dimensions, 4 cm high, 4 cm inner diameter, and 4.3 cm external diameter. Measurements were made at 15, 80, 116, 150, and 180 K at 40 meV incident neutron energy. A mea-

surement at 100 meV and 15 K was also made, which allowed us to cover a momentum transfer range up to 8 Å^{-1}, in the first case and up to 12 Å^{-1}, in the second. Empty can and vanadium normalization runs were also made, and standard multiple-scattering and correction procedures were followed. The resulting data was then unfolded from the effects of resolution by means of a maximum entropy procedure [16].

From the measured double differential cross section the dynamic structure factor $S(Q,\omega)$ is obtained by making use of the standard data reduction package at MARI as,

$$\sigma_{\text{coh}} S(Q,\omega) + \sigma_{\text{inc}} S_S(Q,\omega) = 4\pi \frac{k_0}{k} \frac{d^2\sigma}{d\Omega dE} \tag{1}$$

corresponding to momentum- and energy transfers defined by $\hbar\mathbf{Q}=\hbar(\mathbf{k}_0-\mathbf{k})$, $\hbar\omega=\hbar^2(k_0^2-k^2)/2m$, given in terms of the incident and final wave-vectors and the neutron mass. Notice that the inclusion of both coherent and incoherent parts in the measured cross section arises from the sizeable amount of the latter type of scattering since $\sigma_{\text{coh}}/\sigma_{\text{inc}}=4.533$. Since the single-particle dynamic structure factor $S_S(Q,\omega)$ was known from a previous work [15] a separation of this contribution for the total response enabled us to isolate the coherent response $S(Q,\omega)$. This was a crucial step, specially for the wave vectors well below Q_p [i.e., corresponding to the first maximum in $S(Q)$], where the incoherent response becomes comparable or larger than the coherent one.

Once a corrected estimate for the dynamic structure factor is obtained, several relevant quantities can be computed from the spectra. In particular, estimates for the normalized frequency moments,

$$\langle \omega^n \rangle = \int_{-\infty}^{\infty} d\omega S(Q,\omega)\omega^n / S(Q), \tag{2}$$

with

$$\int_{-\infty}^{\infty} d\omega S(Q,\omega) = S(Q), \tag{3}$$

can be derived from the measured data. The zeroth-frequency moment, which is the quantity that normalizes all the higher order terms simply becomes the $S(Q)$ static structure factor, and the one for $n=2$ can be interpreted in terms of physical frequencies characterizing the propagation of collective excitations. Under the present measurement conditions the 100 meV incident energy runs cover a Q range which stretches up to 12 Å^{-1}, which is exactly the same as that of Champeney *et al.* [6], and is only some 4 Å^{-1} shorter than the one of Garawi, Dore, and Champeney [7].

To allow comparison with spectra calculated for the crystalline solid by means of a lattice dynamical model described in our previous communication, the coherent response was expressed as current-current correlations,

$$J_l(Q,\omega) = \omega^2 S(Q,\omega)/Q. \tag{4}$$

The choice of such a function is motivated by the fact that in the low-damping limit, that is when the ω_Q bare frequencies of the collective excitations are smaller than their Γ_Q damping coefficients, then the maxima in $J_l(Q,\omega)$ may be identified with the $\Omega_Q=(\omega_Q^2+\Gamma_Q^2)^{1/2}$ dressed frequencies which can then be analyzed in terms of velocities of propagating plane waves.

Frequency spectrum

The estimation of a $Z(\omega)$ generalized frequency spectrum can be achieved even if the sample is composed by the coherent-scattering nuclei. In such a case, several alternatives have been proposed in the past [17] which serve to average out the substantial Q dependence readily apparent in the structure factor of such samples. In the present case, we wish to illustrate a route which, apart from enabling the derivation of the frequency distribution, also serves to estimate the multiexcitation contributions on a self-consistent ground. The starting point of the present derivation is constituted by the standard phonon expansion following the incoherent approximation

$$S(Q,\omega) = e^{-2W} \sum_{n=0}^{\infty} \frac{1}{n!} \left[\frac{\hbar Q^2}{6M}\right]^n u_n(\omega), \tag{5}$$

in which the one-phonon term is

$$u_1(\omega) = \frac{Z(\omega)}{\omega}[n(\omega)+1], \tag{6}$$

where W is the Debye-Waller factor, M is the molecular mass, $n(\omega)$ is the occupation number, and $Z(\omega)$ the sought density of states. A normalization condition is established for $u_1(\omega)$, from the expression for the Debye-Waller factor

$$2W = \frac{\hbar Q^2}{6M} \int_{-\infty}^{\infty} d\omega \frac{Z(\omega)}{\omega} n(\omega) = \frac{1}{3}\langle u^2 \rangle Q^2, \tag{7}$$

in which $\langle u^2 \rangle$ is the average atomic mean-square displacement (taken as 0.02 Å^2 for $T=15$ K [15]), so

$$\frac{\hbar}{2M} \int_{-\infty}^{\infty} d\omega u_1(\omega) = \langle u^2 \rangle. \tag{8}$$

If we make a more careful evaluation for the one-phonon term, without making resource to the incoherent approximation, it is still possible to get a simple expression as shown by Buchenau [18]

$$S^{(1)}(Q,\omega) = e^{-2W} \frac{\hbar Q^2}{6M} u_1(\omega) S^{(0)}(Q), \tag{9}$$

in which $S^{(0)}(Q)$ is the elastic structure factor. This is a zero-order approximation as shown by Vineyard [19], which will hold in most of our energy-transfer range, whereas in the low frequency sound-wave regime the term $S^{(0)}(Q)$ should be replaced by an average around Q in a range given by ω/c (c being the sound velocity) which will be narrow enough to make Eq. (9) still valid.

The n-phonon terms are obtained through the convolution

$$u_n(\omega) = \int_{-\infty}^{\infty} d\omega' u_{n-1}(\omega-\omega') u_1(\omega'). \tag{10}$$

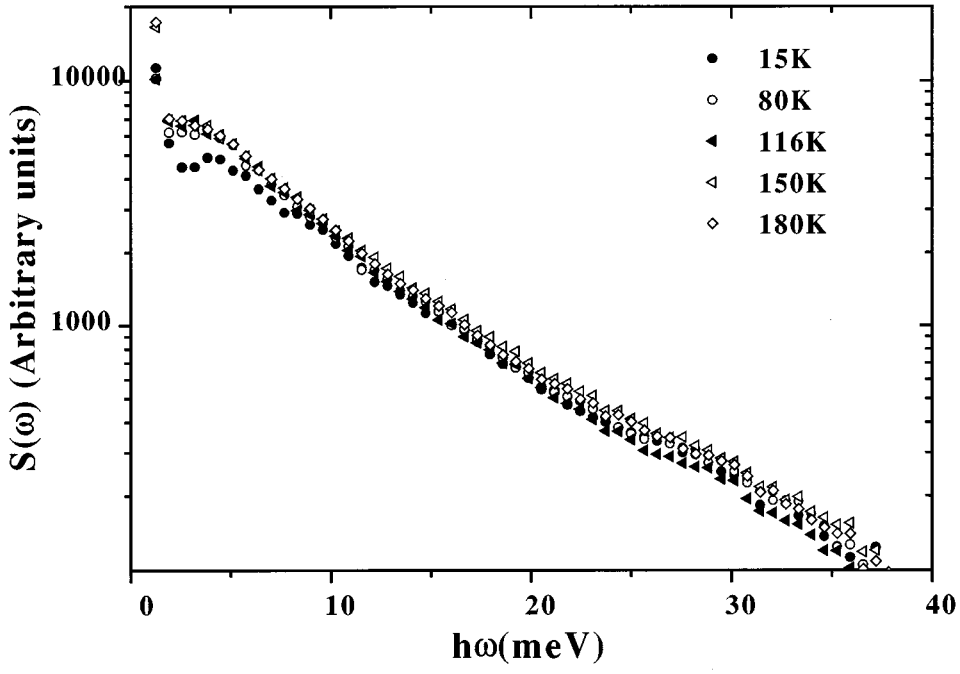

FIG. 1. Experimental data for the energy-transfer kernel at different temperatures, measured with an incident energy of 40 meV.

An energy-transfer kernel is then calculated by taking an average over all measured angles. This averages out the coherent effects and makes the incoherent approximation hold. The resultant expression for such a kernel becomes

$$S(\omega)=\sum_{n=0}^{\infty}\frac{1}{n!}C_n(\omega)u_n(\omega), \tag{11}$$

where $C_n(\omega)$ stands for the angle-average

$$C_n(\omega)=\left\langle e^{-2W(\Phi,\omega)}\left[\frac{\hbar Q^2}{6M}\right]^n\right\rangle_{\Phi}. \tag{12}$$

The data pertaining to $S(\omega)$ at different temperatures is shown in Fig. 1 and corresponds to the set measured using an incident neutron energy of 40 meV. To obtain the density of states from the experimental data, we make use of a recursive calculation, to evaluate the multiphonon terms. In the first step, we use the experimental data as an approximation for the one-phonon term, making use of Eq. (9)

$$K\left\langle\frac{S^{\exp}(Q,\omega)}{e^{-2W(Q)}Q^2S^{(0)}(Q)}\right\rangle_{\Phi}=u_1^{(0)}(\omega), \tag{13}$$

where K is a normalization constant obtained from Eq. (7), and calculate the multiphonon terms from Eq.(10), thus allowing one to define the correction factor $f(\omega)$ as the ratio of the multiphonon terms over the single one

$$S(\omega)=v_1(\omega)+v_m(\omega)=v_1(\omega)[1+f(\omega)], \tag{14}$$

where

$$f(\omega)=\frac{v_m(\omega)}{v_1(\omega)}, \tag{15}$$

$v_1(\omega)$ stands for the one-phonon term, and $v_m(\omega)$ for the total multiphonon contribution. With this factor, we can recalculate u_1 as

$$u_1^{(1)}(\omega)=\frac{u_1^{(0)}(\omega)}{1+f(\omega)}. \tag{16}$$

This process converges after four or five iterations, and becomes comparable in efficiency to the one described in [20] which applies to incoherent-scattering samples only. The final value for u_1 applied in Eq. (6) yields the desired $Z(\omega)$. In Fig. 2 we show the calculated $Z(\omega)$ curves for the different temperatures as measured with 40 meV of incident energy, and in the inset (a), for the scattering data at 15 K and 100 meV incident energy, where we also show the multiphonon contribution. A comparison of the present data with the recently published results on low-frequency inelastic scattering in partially deuterated glycerol [13] seems in order. There, glycerol-D_3 (the OH hydroxyls are deuterated) and glycerol-D_5 (the hydrogens of the methylene CH_2 and CH groups are here substituted by deuterium) are examined, above and below the glass transition, with acceptable statistics within a range of energy transfers up to 20 meV in the anti-Stokes side of the spectra. The main temperature dependent effect of the densities of states given in Ref. [13] regards the onset of quasielastic scattering at temperatures rather close or above T_g which is confined to frequencies below some 4 meV. Within the solid phase such variations are difficult to follow since the rather restricted range of energy transfers and somewhat low-counting rate preclude any direct comparison of data shown in Fig. 4 of [13] with those shown here in Fig. 2, which, as will be discussed with some detail below, are shifted to higher frequencies as the temperature is raised. An extra peak in glycerol-D_3, but not so clear in glycerol-D_5 at approximately 17 meV is also observed in the cited paper. The origin of such a feature can be ascertained from data given in [15], where the single-

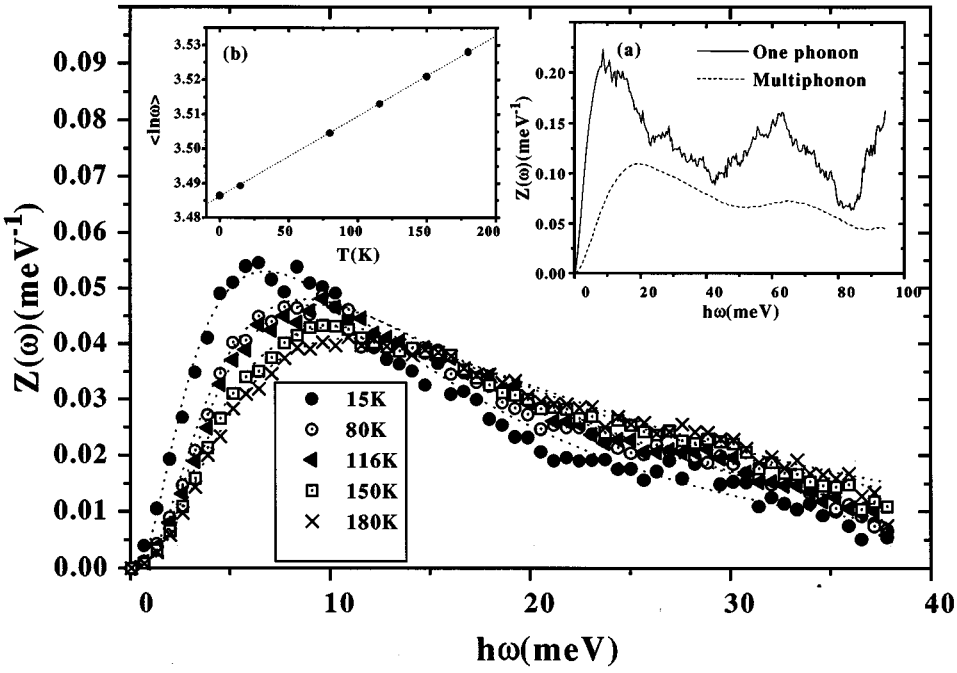

FIG. 2. Calculated densities of states, obtained from the spectra measured with an incident energy of 40 meV. Fitted log-normal curves are indicated with a dashed line. Inset (a): density of states for the spectra at 15 K and 100 meV incident energy, with the multiphonon contribution; inset (b): mean value of $\langle \ln\omega \rangle$ as a function of temperature with a fitted straight line with a slope $\alpha_J = 0.000\ 23\ \mathrm{K}^{-1}$.

molecule internal modes and the effect of their hybridization with lattice modes is discussed. In particular, a calculation of mode eigenvectors for a crystalline solid showed that modes of 16.71 meV and 17.74 meV exhibited large translational and deformational (bond-torsion) components. Since, as we will see below, the dynamics of glass and crystal at these frequency scales share strong similarities, the finding in the crystalline solid should then be relevant for the glass. On the other hand, and on empirical grounds, the fact that such a peak is found in the compound where the CH_2 and CH groups are fully hydrogenated but not in glycerol-D_5 or even in the present experiment, can be accounted for by the fact that in glycerol-D_3 movements involving the CH_2 and CH hydrogens dominate the double differential cross section. Therefore the derived densities of states from the measurement on such samples will weight heavily all the low-frequency bond-torsion motions, whereas measurements where such atoms are substituted by deuterium will show far less prominent contributions from the internal molecular dynamics.

III. RESULTS AND DISCUSSION

In what follows we will describe the results regarding the space-dependent information obtained from the present experiments as well as those regarding those properties derivable from knowledge of the glass frequency distributions such as the thermodynamic functions.

A. Static structure

The $S(Q)$ static structure factor Eq. (3) is directly obtainable from constant-Q integration of $S(Q,\omega)$. Although energy-integrated (diffraction) techniques are in principle better suited to access this kind of information, in some cases such as the present one where the neutron beam produces a substantial vibrational excitation of the molecular internal degrees of freedom, a significant improvement in the reliability of the data can be gained from the analysis of the $S(Q)$ derived from constant-Q (rather than constant-angle) measurements. The reason for this lays in the substantial corrections that need to be applied to the coherent interference pattern [21, 22] (i.e., the experimental phase shifts have to be corrected since the energy-momentum conservation forces the actual Q value to deviate from the elastic one) which require as input the solution of the full molecular vibrational problem. In counterposition, a measurement such as that reported here only needs to account for a smooth correction to the self-terms (i.e., those not leading to interference of the scattered waves) which can be modeled using smooth functions of Q.

The $S(Q)$ so obtained is shown in Fig. 3. For its analysis, recourse was made to the conventional formalism suitable for the molecular materials, where the total diffraction pattern is decomposed into intra- and intermolecular contributions [23]

$$S(Q) = f_M(Q) + D_M(Q); \tag{17}$$

$$f_M(Q) = \sum_{ij} b_i b_j j_0(Q d_{ij}) \exp(-u_{ij}^2 Q^2/2) \left[\sum_i b_i \right]^{-2},$$

where $f_M(Q)$ is a molecular form factor (i.e., a superposition of the j_0 Bessel functions corresponding to d_{ij} interatomic distances between the atom pairs within the molecule, damped by the Debye-Waller terms dependent upon the u_{ij} thermal amplitudes of motions of atoms separated by such distances, and weighted by the b_i coherent scattering lengths), and $D_M(Q)$ stands for the intermolecular structure function which is to be isolated from the total structure factor once an adequate parametric representation for $f_M(Q)$ is found from fits of such a model function to the large-Q portion of $S(Q)$. From there, several geometrical parameters for the molecular configuration can be derived. The interest of such an exercise stems from the observation made from

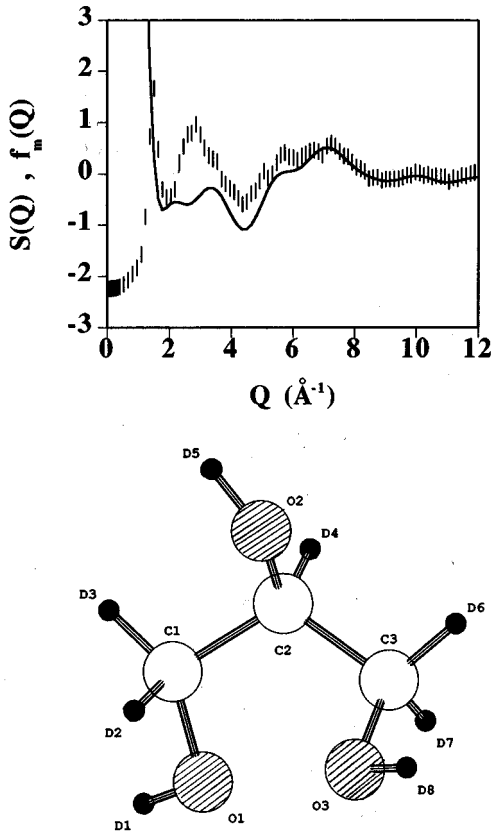

FIG. 3. Experimental structure factor $S(Q)$, along with fitted $f_M(Q)$. See text for details. A sketch of the molecule with the nomenclature for Table I is included.

Raman spectroscopy of the existence within the glass of different molecular isomers, whereas only one (a fully extended molecular configuration) is seen in the crystal diffraction measurements [15].

From the $f_M(Q)$ model fits to the high-Q part of $S(Q)$ [i.e., for $Q \geqslant 7$ Å^{-1} all the intensity in $S(Q)$ is assumed to be originated from short-range, intramolecular correlations], estimates for the molecular parameters were derived and a summary of those is given in Table I. A comparison between the experiment and the model function can be gauged from the graph in Fig. 3, where the resulting equilibrium molecular configuration is also shown. A look at the graph showing the optimal molecular conformation displayed in the same figure evidences a rather distorted structure with respect to that of the crystal which has the form of a flattened ''W'' (i.e., the two oxygens and the three carbons being coplanar in a fully extended configuration).

Some comments regarding the molecular data given in Table I are in order. First and foremost notice that as can be judged from comparison with the two different sets reported by Garawi, Dore, and Champeney [7] and the one of Champeney, Joarder, and Dore [6], the present parameters are now close to those for an equilibrium molecular configuration (i.e., close to the standard reference values for the bond lengths and angles), and therefore should be taken as more reliable than those of Refs. [7] and [6], surely as a consequence of the analysis in terms of the corrected $S(Q)$ achieved through the decomposition procedure that enabled us to isolate intramolecular information. By implication, the intermolecular structure factor should now be more reliable especially regarding the atomic contacts occurring at distances comparable with the molecular dimensions. The molecular configuration reported by Garawi, Dore, and Champeney [7] is different from the present results, mainly as a consequence of having those authors set the parameters specifying the dihedral angles of the second-row molecular skeleton to the same values than those of the crystal, while those reported by Champeney, Joarder, and Dore [6] fail to properly describe the intermolecular contribution to the structure factor, which causes a significant variation with the temperature of the calculated molecular parameters. On the other hand, a comparison with the data of Root and Stillinger [9] regarding a molecular dynamics (MD) simulation for a simplified molecular model (the CH_2 groups are represented as a single pseudoatom), shows that the structure depicted in Fig. 3 is closer to that given as optimal in Ref. [9], although the extent of the intra-molecular hydrogen bonding given in that paper seems overemphasized.

TABLE I. Molecular parameters. Notation is referred to Fig. 3. Bond lengths, and most of the bond angles (i.e., all those values marked with a dagger) were set to the standard reference values. The fitted values for the u_{ij} interatomic mean-square displacements are also shown. Those marked with a dagger correspond to values set to those reported by Garawi, Dore, and Champeney [7]. The mean-square amplitudes refer, in the case of the bond or torsion angles, to those of distances between the outermost atoms.

Bond lengths (Å)	Value	$u_{ij}^2/2 \times 10^3$ Å^2
CC	1.53†	5.4
CD	1.11†	2.3†
CO	1.40†	5.6
OD	0.94†	3.8†
Bond angles (degrees)	Value	
$C_1O_1D_1$	107.3†	10.1†
$C_2O_2D_5$	107.5†	10.1†
$C_1C_2C_3$	115.6	5.6
$C_2C_1D_2$	109.5†	15.†
$C_2C_1O_1$	109.5†	5.4†
Torsion angles (degrees)	Value	
$D_1O_1C_1C_2$	-151.2	20.
$O_1C_1C_2C_3$	-29.1	29.
$D_5O_2C_2D_4$	49.5	17.
$O_3C_3C_2C_1$	-46.2	29.
$D_8O_3C_3C_2$	-130.0	20.

In Fig. 4(a) we show the intermolecular distribution $d_L(r)$ [that is the Fourier transform of $QD_M(Q)$] obtained from our experiment (shown as vertical bars), compared with the liquid structure function taken from Ref. [7] (dash-dotted line), and that resulting from the lattice dynamics (LD) calculations for the crystal [15]. Also indicated are the atom pairings that originate the main peaks in the crystal distribution. We observe that the liquid and glass structure are coincident from r values of some 6 Å on, while some discrepancies can be observed in the short-range region, where some structural details are not seen in the glass probably due to a lower experimental resolution.

The direct correlation function $\rho c(Q) = 1 - 1/D_M(Q)$ is

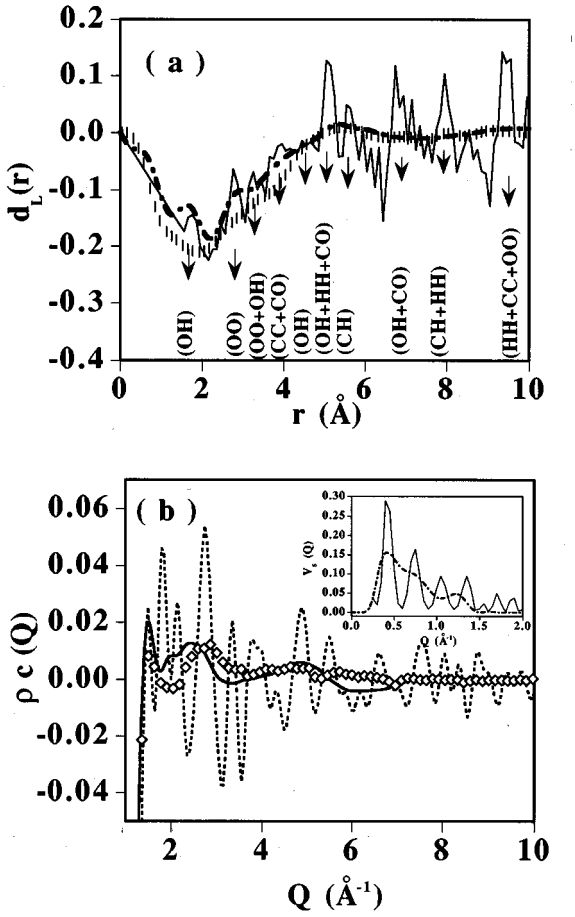

FIG. 4. (a) Intermolecular distributions for the present experiment (vertical bars), liquid (Ref. [7]) and crystal taken from the lattice dynamics calculations with molecular bonds indicated. (b) Direct correlation functions for the glass (lozenges), liquid (full line), and crystal dotted line.

presented in Fig. 4(b), for the glass (lozenges), the liquid [7] (full line) and the crystal [15]. A remarkable result regards the coincidence in position and close agreement in the amplitude of the first peak which appears at $Q_p = 1.49$ Å^{-1} for the three systems, something which goes counter to some attempts to derive significant structural information from such a parameter [11]. In contrast, rather large differences are found regarding the amplitude and position of peaks at a higher Q. In fact, the strong peaks seen in the crystal function at $Q = 1.82 - 2.15$ Å^{-1} are only seen as a shoulder in the liquid data and no definite feature can be identified with them in the curve pertaining to the glass. On the other hand the stronger peak of the crystal function appearing at $Q = 2.75$ Å^{-1} now has a clear analog in the glass phase (albeit broader and with a substantially reduced amplitude), whereas the strong second peak in the liquid function is shifted down by some 0.3 Å^{-1}. In the inset of the same figure we show the quantity,

$$V_s(Q) = \frac{1}{15}\left[D_M(Q) Q \frac{\partial \rho c(Q)}{\partial Q} \right]^2 \qquad (18)$$

which represents the mode-coupling vertex [24] (i.e., amplitude terms which enter the mode-coupling equations as time-independent quantities) for the generalized shear viscosity $\eta_s(Q,z)$, which can be calculated from the knowledge of the direct correlation function. The $V_s(Q)$ shown in the insert displays fine structure reminiscent of that found for the crystal. This result contrasts with the usual hard sphere models normally applied in current theoretical approaches to real liquids.

B. Space-dependent motions

From the lattice dynamics model developed in our previous communication [15] the $S(Q,\omega)$ dynamic structure factor was calculated for the harmonic solid after an orientational averaging was made within the Brillouin zone and the Debye-Waller was set to that observed at $T = 15$ K. The spectral frequency distribution of such a model crystal stretches up to ≈ 60 meV as a consequence of the lowest-laying internal molecular modes which need to be accounted for to reproduce the crystal thermodynamics at temperatures close to T_g [15]. However, inspection of the dispersion branches corresponding to the highest symmetry directions showed evidence that excitations with a strong wave-vector-dependence are confined to frequencies below 7 meV. Above that, most branches are dispersionless. To quantify this, and to provide a reference for the Q-dependent frequency distributions in the glass, Fig. 5 shows some $J_l(Q,\omega)$ functions calculated for the polycrystal and for the glass. To extend the kinematic range as much as possible, spectra for the same Q values were taken from the 40 meV and 100 meV incident energy runs. As seen from Fig. 5, a combination of spectra from these two experiments serve to cover the required range in the energy transfers without degrading the finite-frequency details to an unbearable extent. The elastic peaks which for this low temperature were basically δ functions, were subtracted from the reconstructed (unfolded) spectra which were derived following the procedures mentioned above. Such a step was a necessary one to carry since the tails of the resolution-broadened elastic peak would contribute substantially to $J_l(Q,\omega)$.

As can readily be seen from graphs drawn in Fig. 5, at the lower Q values (up to 1 Å^{-1}) the main difference between crystal and glass spectra regards a substantial intensity in the spectra of the latter at low (below some 2 meV) frequencies. Also, the first maximum of $J_l(Q,\omega)$ appears slightly downshifted with respect to the crystal. In opposition, above some 1 Å^{-1} the spectra of the glass and the polycrystal are very similar, especially with respect to the peak position, although the peak in the glass spectra is broader. These general trends regarding the differences between the glass and the polycrystal have also been seen in a comparison between liquid and polycrystal methanol [25], and can be rationalized in terms of recent results from the density functional theories of freezing [26].

To quantify these differences between both sets of spectra, the square root of the second normalized frequency moment is shown in Fig. 6. The straight line drawn in the figure corresponds to the sound waves traveling with a phase velocity of 3900 m s^{-1}, (extrapolated from the experimental ultrasound data for the glass by Litovitz and Lyon [27]). A comparison between the hydrodynamic dispersion law calculated using the ultrasound data and the second frequency

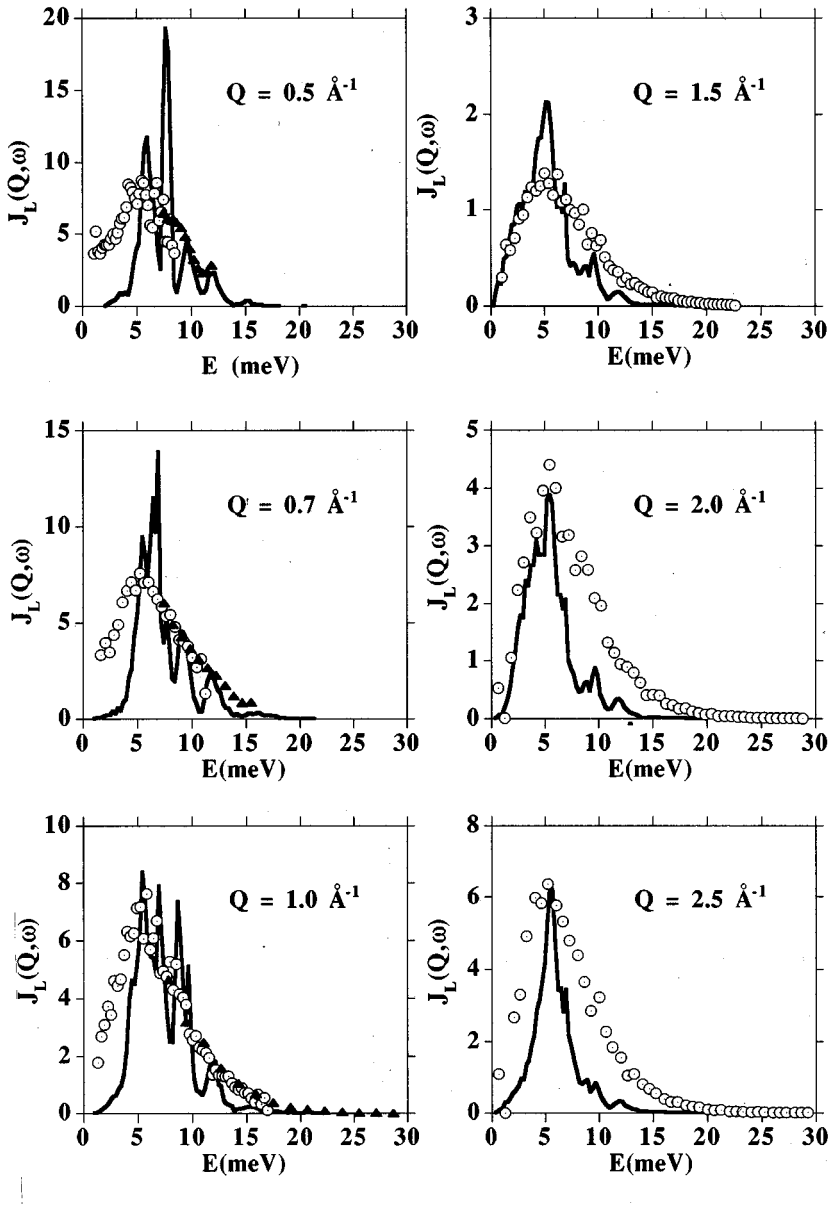

FIG. 5. $J_l(Q,\omega)$ for the polycrystal from the LD calculation compared with the measured corresponding values for the glass at 15 K with 40 meV incident energy (circles) and 100 meV (full triangles), at different Q values shown in the insets.

moments for the glass and crystal evidences that,

(i) The linear dispersion evidenced by the crystal $\langle\omega^2\rangle^{1/2}$ below 0.3 Å^{-1} corresponds to a velocity of some 2960 m s^{-1}. This is well below that given above for the longitudinal acoustic excitations measured for the glass, but comes reasonably close to the estimate of 2635 m s^{-1} derived from an orientational averaging of longitudinal and transverse sound speeds given in Ref. [15]. In consequence, and within such a limited range of Q, the crystal $\langle\omega^2\rangle^{1/2}$ can rightly be interpreted in terms of an average physical frequency describing the propagation of sound waves.

(ii) The second frequency moment for the glass becomes substantially smaller than those of the crystal below some 1 Å^{-1} as a consequence of the contribution of low-frequency modes in the glass data. Consequently it seems difficult to assign a definite physical meaning to a parameter such as $\langle\omega^2\rangle^{1/2}$ than that of its usefulness to describe a frequency distribution.

(iii) Alternatively, a comparison between the glass and crystal data may also be carried in terms of frequencies corresponding to the peak maxima in $J_l(Q,\omega)$; these are the dressed frequencies Ω_Q referred to above. If this is done, then as shown in Fig. 6 frequencies far closer to those where the crystal shows their maxima are found.

In summary, what becomes clear from the present work is that the hydrodynamic region, where sound excitations are expected to follow a linear dispersion law, would be confined for the glass to a region below 0.1 Å^{-1}. This is a region which is difficult to observe using conventional neutron instrumentation, and even with present day inelastic x-ray scattering techniques.

C. Thermodynamics

The constant-pressure specific heat $C_p(T)$, is calculated in the quasiharmonic approximation from [28]

$$C_P^{qh}(T)=GR\int_{-\infty}^{\infty}d\omega Z(\omega,T)\frac{x^2}{\sinh^2 x}, \tag{19}$$

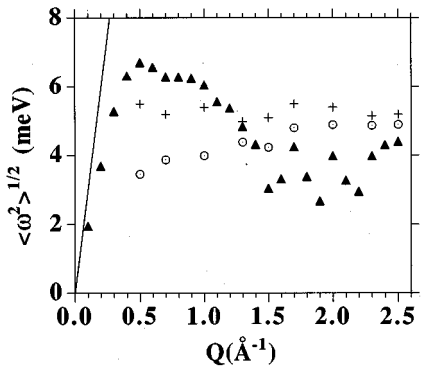

FIG. 6. Calculated (square root of the) second normalized frequency moments for the crystal (LD calculation, full triangles) and measured for the glass at 15 K (circles). The line corresponds to the sound dispersion curve for the glass extrapolated at this temperature, and crosses indicate the position of the maxima in the $J_l(Q,\omega)$ for the glass.

with $x=\hbar\omega/2k_BT$, R being the gas constant, and G is the number of degrees of freedom. The first-order anharmonic correction, is given from the temperature dependence of the frequency distributions following,

$$\Delta C_P^{\mathrm{anh}}(T)=-GR\int_{-\infty}^{\infty}d\omega Z(\omega,T)\frac{x^2}{\sinh^2 x}\left[\frac{\partial\ln\omega}{\partial\ln T}\right]_P, \tag{20}$$

where the $Z(\omega,T)$ temperature-dependent densities of states is shown in Fig. 2. Following the suggestion of Malinovsky *et al.* [29], the neutron densities of the states were analyzed in terms of a log-normal function (see Fig. 2),

$$Z(\omega,T)=\exp\left[-\frac{1}{2}\left(\frac{\ln[\hbar\omega/a_1(T)]}{a_2(T)}\right)^2\right], \tag{21}$$

where $a_1(T)$ and $a_2(T)$ are adjustable parameters. The width $a_2(T)$ was found to be essentially constant, whereas the centroid $a_1(T)$ showed a linear dependence given by $a_1(T)=6.85(1+0.0038T)$. The errors obtained from those fittings range from 3% in the low-energy limit up to 6% at 40 meV. Also, data regarding the temperature dependence of the Raman spectra discussed in a previous paper [15], were used to characterize the anharmonic effects for the higher frequencies. Raman spectra, which were taken at seven different temperatures ranging from 8 to 190 K, showed a characteristic low frequency peak (with a maximum at ≈ 8 meV), and strongly marked peaks at ≈ 52, 61, 68, and 83 meV, as can be observed in Fig. 2 of Ref. [15]. Those high-frequency peaks were fitted to Gaussians whose centroid was also observed to exhibit a decrease in frequency varying linearly with temperature. After collecting all the above mentioned data, it was found that the spectral-frequency dependence with temperature could be written as,

$$\hbar\omega=\hbar\omega_0[1+\beta_J(\omega)T], \tag{22}$$

with $\beta_J(\omega)=0.004\,05\exp[-(\hbar\omega/30)^2]$, where the energies are given in meV. It was also found that the mean value of the logarithm of the frequencies, varies linearly with the logarithm temperature

$$\left[\frac{\partial\langle\ln\omega\rangle}{\partial\ln T}\right]_P=\alpha_J T \tag{23}$$

with $\alpha_J=0.000\,23\ \mathrm{K}^{-1}$, as can be seen in the inset (b) of Fig. 2.

Taking into account these parameters, $Z(\omega,T)$ can be expressed by reference to the zero-temperature extrapolated expression, as

$$Z(\omega,T)=Z\left(\frac{\omega}{1+\beta_J(\omega)T},0\right). \tag{24}$$

We used the $Z(\omega,T)$ measured at 15 K and 100 meV incident energy as the reference, because of its wider energy range, and applied the effective frequency transformation given in Eq. (22) [as expressed in Eq. (24)] as a simple way to fully describe the temperature behavior of the density of states.

The complete expression for the specific heat is calculated from Eqs. (25) and (20), in which the derivative of $\ln\omega$ with respect to $\ln T$ is taken in the effective way expressed in Eq. (23), so

$$C_P(T)=GR\int_{-\infty}^{\infty}d\omega Z\left(\frac{\omega}{1+\beta_J(\omega)T},0\right)\frac{x^2}{\sinh^2 x}\,\frac{1-\alpha_J(T)}{A(T)}, \tag{25}$$

where $A(T)$ is an area renormalization constant for $Z(\omega)$, which varies as $A(T)=1+0.000\,15T$.

In Fig. 7, we show the total C_P value, as well as the quasiharmonic approximation compared with the experimental calorimetric results [1]. A value of 20 was chosen for G, so that the quasiharmonic expression approaches 20 R in the high temperature limit, which is well beyond the glass transition. The errors in the evaluation of the specific heat range from 4% at 15 K up to 7% at 150 K. In the inset of the same figure, we show the anharmonic correction for C_V. The fitted straight line in this graph shows the behavior of $\Delta C_V^{\mathrm{anh}}$.

$$\frac{\Delta C_V^{\mathrm{anh}}}{GR}=A(V)T=-1.260\times10^{-4}T \tag{26}$$

which constitutes a good estimate of the leading order term $[A(V)]$ in the temperature expansion of the anharmonic correction for the specific heat and the entropy.

It is also interesting to assess the temperature dependence of the Grüneisen parameter, to relate it to the system anharmonicity

$$\gamma=\frac{\beta V K_T}{C_V}, \tag{27}$$

where β is the volume coefficient of the thermal expansion, and K_T the isothermal bulk modulus of elasticity. We can express it also in relation to the jth independent contributions to the specific heat as

$$\gamma C_V=\sum_{j=1}^{n}\gamma_j C_j \tag{28}$$

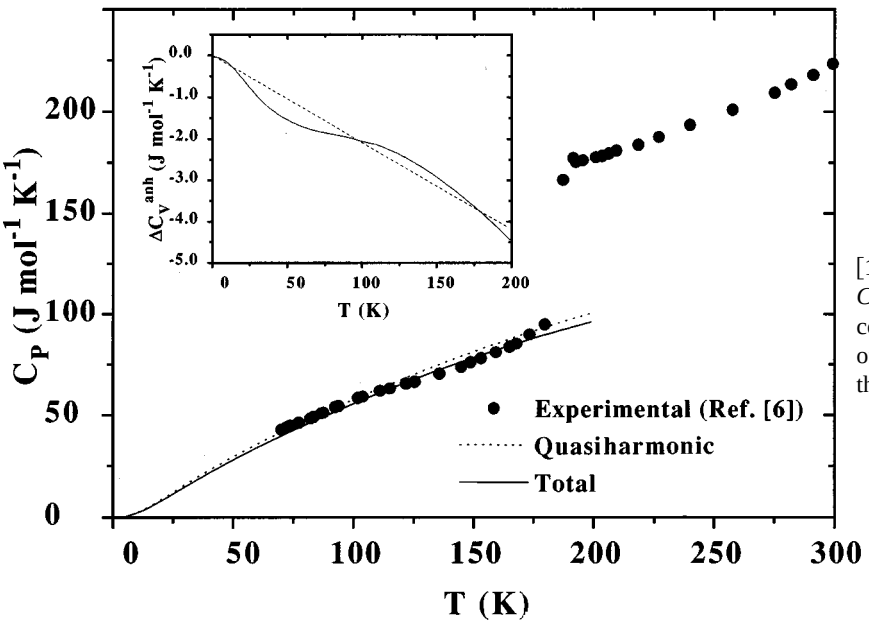

FIG. 7. Experimental C_P values from Ref. [1], compared with the calculation for the total C_P according to Eq. (25) and its quasiharmonic contribution. Inset: the full line shows the detail of the anharmonic correction and the dotted line the fitted linear relation from Eq. (26).

from which we may separate it as a quasiharmonic and an anharmonic contribution [30]

$$\gamma C_V = \gamma^{qh} C_V^{qh} + \gamma^{\mathrm{anh}} C_V^{\mathrm{anh}}. \tag{29}$$

We evaluated γ and γ^{qh} from the thermodynamic parameters extracted from Ref. [27] and also the γ^{anh}, which is shown in Fig. 8. The range of temperatures in which the data are presented corresponds to that in which the thermodynamic parameters were available. We were also able to evaluate the volume variation of *A(V)*, through the relation

$$\frac{A(V)}{A(V_0)} = \left(\frac{V}{V_0}\right)^{\gamma_{\mathrm{anh}}}, \tag{30}$$

which is shown in the inset of the same figure. We observe that its variation in the glass temperature range is in the order of one per thousand.

IV. CONCLUSIONS

By means of an inelastic neutron scattering experiment on glassy D glycerol we were able to study its static structural aspects, as well as its main collective dynamical features. From the structural point of view, we obtained a set of parameters defining the molecular geometry in the glassy state, which differs from that of the crystal, stressing the fact made out from the Raman experiments on the existence of different monomers in the glassy state. Some meaningful observations on the intermolecular structure could also be extracted. No significantly large differences in the short-range intermolecular structure between liquid and glass were found, and as a matter of fact, even the reduction in ''correlation length'' upon melting the glass is remarkably modest ($\approx$17 Å in the glass versus $\approx$15 Å for the liquid [5]).

The coincidence in the position of the first peak in the $\rho c(Q)$ direct correlation function for the crystal, the liquid,

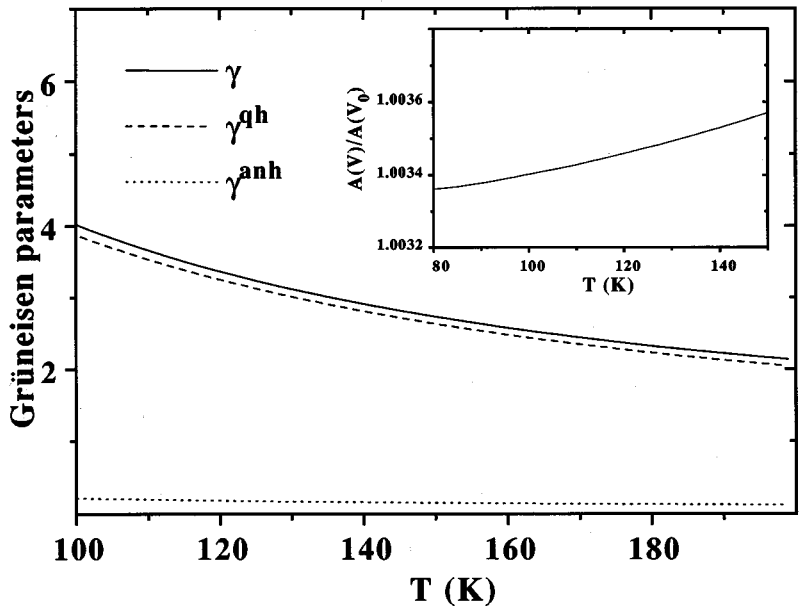

FIG. 8. Grüneisen parameter γ, and its quasiharmonic and anharmonic contributions. Inset: the relative variation of the leading term in the anharmonic expansion of the specific heat *A(V)*.

and the glass seems of special relevance in the light of the present debates about the physical meaning of the parameters characterizing the first diffraction peak and follows that found for some archetypal glasses (silica [32]) which have been recently reexamined in the light of a pseudocrystalline model. The present results show that the significant differences in the long-range order between the three systems do not translate into substantial changes in the parameters regarding the first peak but rather in peaks and valleys at higher momentum transfers.

Comparison of the dynamical information derived for the glass by experimental means and that corresponding to the crystal from the LD calculation, showed that many features regarding excitations of lattice origin are still present in the glass phase. As a matter of fact, comparison of the wave-vector-dependent frequency distributions as represented by the $J_l(Q,\omega)$ correlation functions, show that apart from the far broader shape of that functions for the glass, the main difference regards a redistribution of spectral power towards lower frequencies which become rather evident for the glass for wave-vectors below some 1 Å^{-1}. Above such momentum transfers, the Q-dependent frequency distributions become comparable as judged by the second reduced frequency moment. The similarity of shapes of $J(Q,\omega)$ of the crystalline powder and the glass shown in Fig. 5 seems to lend some support to results from the density functional theory of freezing [26], where the characteristic shapes of phonon spectra in a hot crystal are shown to be related to that of the normal liquid. Such relationships between the spectra of powder and glass are also reminiscent of those recently expressed by Wolf *et al.* [33] in a computer simulation of a material in glassy and nanocrystalline forms.

Starting from the microscopic data obtained from our neutron scattering data, we were able to perform a calculation of the constant pressure specific heat, as well as a detailed evaluation of the anharmonic contribution, through a temperature parametrization of the densities of states obtained in combination with Raman scattering data. A good agreement with calorimetric data on the glassy phase was obtained. Further thermodynamic calculations were carried out, especially the leading order term in the anharmonic correction of the entropy *A(V)* (observed to be almost constant), which is negative and in the same order of magnitude observed in crystals [31] (e.g., -1.0×10^{-4} K^{-1} for lead, and -1.9×10^{-5} for aluminum).

ACKNOWLEDGMENTS

Work supported in part by Grant No. PB92-0114-c03-01 (Spain). J.D. wishes to thank CONICET (Argentina) and CSIC (Spain) for financial support.

[1] M. Rajeswari and A.K. Raychaudri, Phys. Rev. B **47**, 3036 (1993).
[2] N.O. Birge, Phys. Rev. B **34**, 1631 (1986).
[3] M. Massalska-Arodz, Phys. Rev. B **43**, 13 676 (1991).
[4] W. Tandy Grubbs and R.A. Mc Phail, J. Chem. Phys. **100**, 2561 (1994).
[5] S. Kojima, Phys. Rev. B **47**, 2924 (1993).
[6] D.C. Champeney, R.N. Joarder, and J.C. Dore, Mol. Phys. **56**, 337 (1986).
[7] M. Garawi, J.C. Dore, and D.C. Champeney, Mol. Phys. **62**, 475 (1987).
[8] H.J.M. Honley, G.C. Straty, C.G. Glinka, and J.B. Hayter, Mol. Phys. **62**, 1165 (1989).
[9] L.J. Root and F.H. Stillinger, J. Chem. Phys. **90**, 1200 (1989).
[10] This regards some assumptions concerning constraints imposed to the molecular structure when fitting the high-Q portion of the dynamical structure factor $S(Q)$, applied in diffraction experiments in order to reduce the number of parameters describing the molecular structure as well as the inelastic contributions.
[11] A.P. Sokolov, A. Kisliuk, M. Soltwisch, and D. Quitmann, Phys. Rev. Lett. **69**, 1540 (1992).
[12] J. Wuttke, J. Hernandez, G. Li, G. Coddens, H.Z. Cummins, F. Fujara, W. Petry, and H. Sillescu, Phys. Rev. Lett. **72**, 3052 (1994).
[13] J. Wuttke, W. Petry, G. Coddens, and F. Fujara, Phys. Rev. E **52**, 4026 (1995).
[14] N. Menon and S.R. Nagel, Phys. Rev. Lett. **74**, 1230 (1995).
[15] F.J. Bermejo, A. Criado, A. de Andres, E. Enciso, and H. Schober, Phys. Rev. B **53**, 5259 (1996).
[16] F.J. Bermejo, F. Batallán, E. Enciso, M. García-Hernández, J. Alonso, and J.L. Martínez, Europhys. Lett. **12**, 129 (1990).
[17] See, for example, J.B. Suck and H. Rudin, in *Glassy Metals II*, Vol. 53 of *Topics in Applied Physics* (Springer-Verlag, Berlin, 1983), Chap. 7, p. 217; J.M. Carpenter, C.A. Pelizzari, Phys. Rev. B **12**, 2391 (1975); **12**, 2397 (1975).
[18] U. Buchenau, Z. Phys. B **58**, 181 (1985).
[19] G.H. Vineyard, Phys. Rev. **110**, 999 (1958).
[20] V.F. Sears, Phys. Rev. A **7**, 340 (1973); J. Wuttke, M. Kiebel, E. Bartsch, F. Fujara, and W. Petry, H. Sillescu, Z. Phys. B **91**, 357 (1993).
[21] J.G. Powles, Mol. Phys. **36**, 1161 (1978); **36**, 1181 (1978), and references therein.
[22] P.E. Egelstaff, in *Methods of Experimental Physics*, edited by D.L. Price and K. Sköld (Academic, San Diego, 1987), Vol. 23B, p. 428.
[23] For a description in some detail see M. Alvarez *et al.*, Mol. Phys. **66**, 397 (1989).
[24] M.C. Marchetti, Phys. Rev. A **33**, 3363 (1986).
[25] J. Alonso, F.J. Bermejo, M. García-Hernández, J.L. Martínez, W.S. Howells, and A. Criado, Phys. Lett. A **172**, 177 (1992).
[26] M.P. Tosi and V. Tozzini, Philos. Mag. B **69**, 833 (1994).
[27] T.A. Litovitz and T. Lyon, J. Accou. Soc. Am. **30**, 856 (1958).
[28] J.C.K. Hui and P.B. Allen, J. Phys. C **8**, 2923 (1975).
[29] V.K. Malinovsky, V.N. Novikov, P.P. Parshin, A.P. Sokolov, and M.G. Zemlyanov, Europhys. Lett. **11**, 43 (1990).
[30] B. Yates, *Thermal Expansion* (Plenum, New York, 1992).
[31] A.J. Leadbetter, J. Phys. C **1**, 1489 (1968).
[32] P.H. Gaskell and D.J. Wallis, Phys. Rev. Lett. **76**, 66 (1996).
[33] D. Wolf, J. Wang, S.R. Phillpot, and H. Gleiter, Phys. Lett. A **205**, 274 (1995).